ARTICLE

Characteristic activity of phosphorous acid in the dehydration condensation of a chitin-derived nitrogen-containing sugar alcohol

Received 00th January 20xx,
Accepted 00th January 20xx

DOI: 10.1039/x0xx00000x

Cheng Yang,[a,b] Takuya Sagawa[a,c], Atsushi Fukuoka*[a] and Hirokazu Kobayashi*[a]

Chitin is a potential resource for the production of renewable organonitrogen compounds, as it contains biologically fixed nitrogen. Hydrolysis of chitin followed by hydrogenation gives the sugar alcohol named 2-acetamido-2-deoxysorbitol (ADS). The dehydration condensation of ADS produces 2-acetamido-2-deoxyisosorbide (ADI), which is a prospective precursor to nitrogen-containing polymers. However, the conversion of ADS to ADI in previous works needed a large amount of CF_3SO_3H as a superstrong acid catalyst, which offered high cost and special corrosion-resistant equipment. In this work, we have found that H_3PO_3, a weak acid, can convert ADS to ADI. Possibly, H_3PO_3 alters the reaction mechanism from the simple acid-catalysed dehydration cyclisation to the cyclisation via phosphite esters. Density functional theory calculations suggest that the modified pathway via the phosphite esters significantly reduces the activation energy. In addition, the reducing ability of the acid likely decreases the formation of condensation by-products.

Introduction

Chitin is a plentiful biomass produced by terrestrial and marine organisms at a rate of ca. 100 billion tons annually.[1] Currently, a major source of chitin is shell waste discharged from the fisheries, and the chitin amount contained in the waste is two to three million tons.[2] This compound is a polymer of *N*-acetylglucosamine (NAG) (Fig. 1), and more than half of the nitrogen atoms come from the natural nitrogen fixation by microbes such as rhizobia. Therefore, chitin will be a renewable resource suited for the production of particular organonitrogen compounds without using ammonia synthesized in the energy-consuming Haber-Bosch process.[2,3]

Hydrolysis of chitin to NAG, the primary intermediate for the production of chemicals, has been studied over the years. A typical method is the chemical hydrolysis using a large amount of concentrated acid (substrate/acid < 1 mol-monomer/mol),[4] which is not a catalytic condition. To improve the efficiency, mechanochemical approaches[5-8] and molten salt systems[9] have been proposed recently. These reactions allow the hydrolysis of chitin to NAG using catalytic amounts of acids.

The conversion of NAG has produced potentially useful chemicals. 3-Acetamido-5-acetylfuran (3A5AF) and chromogens are representative examples in the derivatives of NAG,[10-12] as they may become platform chemicals for aromatics.[13,14] Another attractive compound would be 2-acetamido-2-deoxysorbitol (ADS), which forms by the hydrogenation of NAG (Fig. 1).[6,15] We reported the synthesis of 2-acetamido-2-deoxyisosorbide (ADI) as an ADS-derived potential precursor to nitrogen-containing polymers such as polyamides.[16] Notably, ADI has condensed five-membered rings with one hydroxy and one acetamido group. The rigid framework may provide good properties to polymers.[17] This is because a diol compound having the same skeleton (isosorbide) is a monomer for the commercial polycarbonate named Durabio, an engineering plastic.[18,19] The polymer shows good scratch resistance, high impact resistance and outstanding transparency. Hence, ADI-derived polymers might have similar advantages.

The attractive nature of ADI motivated us to focus on its efficient production. The synthesis involves a two-step dehydration condensation of ADS via 1,4-anhydro-ADS or 3,6-anhydro-ADS (Fig. 1). This reaction required a large amount of CF_3SO_3H as a catalyst in previous reports.[16,20] Density functional theory (DFT) calculations indicated that the oxygen atom in the acetamido group of ADS works as a base to quench acid catalysts. Therefore, a large amount of strong acid was needed to overcome the levelling effect. However, we should develop more economical and less corrosive catalysts to be feasible in chemical processes. Thus, in this work, we explored weak acid catalysts that can convert ADS to ADI, and found that phosphorous acid (H_3PO_3) characteristically shows high activity in this reaction. Our experimental and theoretical

[a] *Institute for Catalysis, Hokkaido University, Kita 21 Nishi 10, Kita-ku, Sapporo, Hokkaido 001-0021, Japan. E-mail: kobayashi.hi@cat.hokudai.ac.jp (H.K.); fukuoka@cat.hokudai.ac.jp (A.F.)*
[b] *Graduate School of Chemical Sciences and Engineering, Hokkaido University, Kita 13 Nishi 8, Kita-ku, Sapporo, Hokkaido 060-8628, Japan.*
[c] *Department of Industrial Chemistry, Faculty of Engineering, Tokyo University of Science, 12-1 Ichigayafunagawara-machi, Shinjuku-ku, Tokyo 162-0826, Japan.*
†Electronic Supplementary Information (ESI) available: [details of any supplementary information available should be included here]. See DOI: 10.1039/x0xx00000x

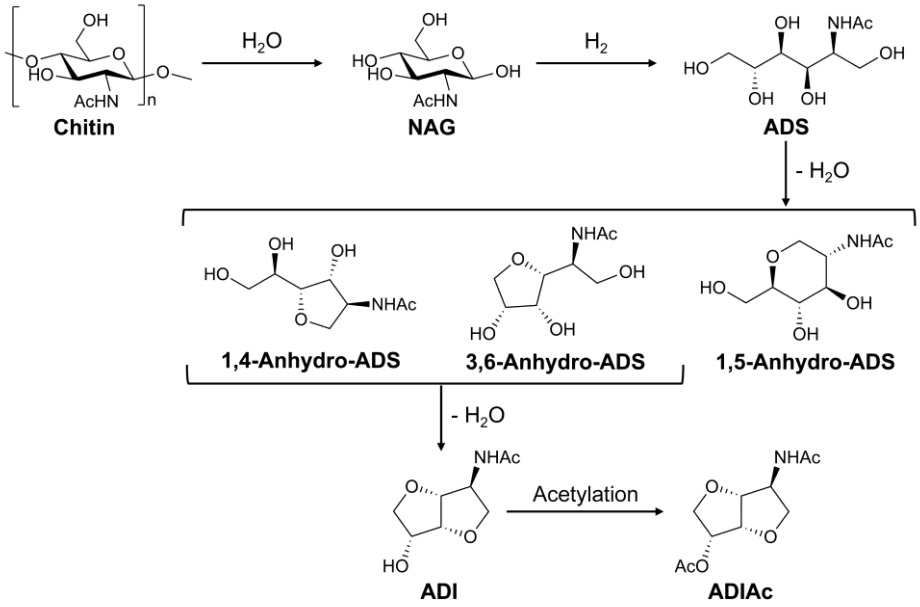

Fig. 1 Reaction pathway from chitin to ADI. One unit of chitin contains 6.9 wt% of N theoretically. Some of monomer units in chitin do not have acetyl groups.

studies have indicated that H_3PO_3 promotes the reaction via phosphite esters, which is a different mechanism from that for strong acids.

Experimental

Reagents. NAG (>95%), methanol, HCl aq. (35%), H_2SO_4, oxalic acid, H_3PO_4 aq. (85%), acetic acid and dl-malic acid were purchased from Fujifilm Wako Pure Chemical. Ru/C (Ru metal loading 5.0 wt%) and H_3PO_3 were supplied from Sigma-Aldrich. CF_3SO_3H, dimethyl phosphite, diethyl phosphite and diisopropyl phosphite were obtained from Tokyo Chemical Industry. 2,4-Dinitrobenzonic acid (2,4-DNBA) was received from Alfa Aesar.

Synthesis of ADS from NAG.[16] NAG (1.6 g) and Ru/C (1.0 g) were added in water (40 mL), and the mixture was pressurised with H_2 (4 MPa). After keeping at 80 °C for 1 h, the mixture was filtered with a mixed cellulose ester membrane (Advantec, 25AS045AN, 0.45 µm pores) and condensed under a reduced pressure to make it almost solid. The product was dissolved in methanol (40 mL) and stored at −30 °C for recrystallisation. ADS was obtained as solid (1.1 g, 65% yield from NAG).

Conversion of ADS by acid catalysts. An acid catalyst and ADS (112 mg, 0.5 mmol) were dissolved in H_2O (0.2 mL) in a Schlenk tube (Kanto Chemical, 20 mL). A typical substrate/catalyst (S/C, mol/mol) ratio was 2.0. The reactor was connected to a rotary pump via a trap immersed in liquid N_2. Then, the mixture was dried under reduced pressure (<0.1 kPa) overnight to completely remove water. Under the reduced pressure or atmospheric pressure, the apparatus was immersed in a pre-heated oil bath and kept for a certain time at a determined temperature (e.g., 150 °C for 3 h).

Product analysis. After adding 10 mL of water to the product mixture, soluble products were analysed with a high-performance liquid chromatograph (HPLC; Shimadzu LC-20AD) equipped with a Rezex RPM-Monosaccharide Pb++ column (Phenomenex, 300 × ø7.8 mm, 70 °C) and a refractive index detector (RID). Water (0.6 mL min^{-1}) was used as the mobile phase. Size exclusion chromatography (SEC) analysis was conducted using an HPLC (Shimadzu, LC-20AR) equipped with two GF-210 HQ columns in a row (Shodex, 300 mm × ø7.5 mm, 50 °C) and an RID. An aqueous solution of 0.02 mol L^{-1} acetic acid was used as an eluent at a flow rate of 0.5 mL min^{-1}. The liquid chromatography-mass spectroscopy (LC/MS) was performed using a Shimadzu LC-20AR HPLC system equipped with a Shodex Sugar SH-1011 column and an LCMS-2020 mass spectrometer. The MS consisted of an electrospray ioniser (ESI) and a quadrupole mass analyser.

Proton decoupled phosphorus nuclear magnetic resonance (NMR; ^{31}P 243 MHz) was measured on a JEOL ECX-600 spectrometer using 85% H_3PO_4 as an external standard. Ultraviolet-visible (UV-Vis) spectra of the products were measured on a JASCO V-650 at a scan rate of 400 nm min^{-1} using quartz cells with an optical path length of 10 mm. Samples were diluted 10 times with distilled water before the measurements.

DFT calculations of reaction pathway. We used the Gaussian 16 software program for the DFT calculations at the B3LYP/6-31+G(d, p) level to determine energy profiles of the conversion of ADS.[21-25] The solvation effect was involved by the solvation model based on density (SMD)[26] with using *N*,*N*-dimethylformamide to reproduce the effect of acetamido groups. Each transition state found had only one imaginary number vibration frequency, and the intrinsic reaction coordinate (IRC)[27] connected the reactant and the expected product.

NMR chemical shift prediction. Chemical shift values (δ) in ^{31}P NMR were predicted by eq. 1, where σ_{calc} is a computed

isotropic shielding constant (see below). The coefficients *a* and *b* were determined by the least-squares fitting method using the chemical shift values obtained by actual NMR measurements and the σ_{calc} values of the commercially available phosphite esters, specifically dimethyl phosphite, diethyl phosphite and diisopropyl phosphite.

$$\delta_{pred} = a\sigma_{calc} + b \quad (1)$$

To determine σ_{calc} of a compound, the effect of multiple conformations was included based on the thermodynamic distribution. Possible conformations of a compound were systematically made with the molclus software,[28] and their geometry was optimised at the B3LYP/6-31+G(d,p) level on Gaussian 16.[29] After excluding unstable conformations that do not contribute to σ_{calc}, more accurate energy and isotropic shielding constant for each structure were determined in a single point calculation at the B3LYP/6-311+G(d,p) level with the Gauge-Independent Atomic Orbital (GIAO) method.[30,31] The functional accurately predicts the shielding constant of phosphorus, according to the literature.[32] Suppose we obtained *n* conformations that should be considered, the existence ratio of a specific conformation (number *k* within *n*) to the most stable one (number 1), denoted K_k, can be estimated using an energy difference between the two conformations as eq. 2, where *e* is Napier's constant, *R* the gas constant, and *T* an ambient temperature (298 K). Finally, σ_{calc} was defined as their existence ratio-weighted average of the shielding constants (eq. 3).

$$K_k = e^{-\frac{E_k - E_1}{RT}} \quad (2)$$

$$\sigma_{calc} = \frac{\sum_1^n K_k \sigma_k}{\sum_1^n K_k} \quad (3)$$

Results and discussion

The dehydration condensation of ADS was performed with acid catalysts (S/C = 2.0) at 150 °C under atmospheric pressure. The reaction pathway from ADS to ADI includes a two-step dehydration reaction as shown in Fig. 1.[16] The first dehydration converts ADS to 1,4-anhydro-ADS, 3,6-anhydro-ADS and 1,5-anhydro-ADS. 1,4-Anhydro-ADS and 3,6-anhydro-ADS undergo the second dehydration to give ADI, while 1,5-anhydro-ADS is a by-product. In addition, acetylation of ADI gives 6-*O*-acetyl-ADI (denoted ADIAc).[20] We have clarified that the rate-determining step is the dehydration of 1,4- and 3,6-anhydro-ADS to ADI.[16] As shown in Table 1 (entry 1), a reaction with no acid catalyst converted ADS to mono-anhydrides in 28% yield in total, but catalysts were essential for the second dehydration to form ADI. Strong acids – CF_3SO_3H, HCl and H_2SO_4 – gave ADI in 11–19% yield, monoanhydro ADS and ADIAc (entries 2–4). A large amount of unidentified by-products, most likely deacetylated compounds and humins, were also formed (49–67%). These results follow the previous literature.[16] Then we tested various weak acids with pK_a values of 1.2–2.8 (oxalic acid, H_3PO_3, 2,4-DNBA, H_3PO_4 and malic acid) (entries 5, 6, 9–11). Among them, H_3PO_3 gave the highest yield of ADI (19%, entry 6), and surprisingly this yield was as high as that given by CF_3SO_3H (19%, entry 2). This result is apparently contradictory to our previous report on a low activity of H_3PO_3,[16] but the difference is due to the solvent used for the impregnation of H_3PO_3 on ADS. The use of diethyl ether in the previous work led to a low yield of ADI (5.3%, entry 7), whereas water resulted in 19% yield of ADI (entry 6). A possible reason is impurities in diethyl ether such as peroxides, stabiliser and oxidised stabiliser. For example, peroxides may oxidise H_3PO_3 to H_3PO_4. To avoid the negative influences of the impurities, water should be used as a solvent in the impregnation process. After the optimisation of reaction parameters using H_3PO_3 (details: Table S1), the

Table 1 Dehydration of ADS by acid catalysts with different pK_a values.[a]

Entry	Catalyst	pK_a	Conv. /%	Yield of product /%					
				ADI	1,4-AHADS[b]	3,6-AHADS[b]	1,5-AHADS[b]	ADIAc	Others
1	None	-	54	<0.1	15	3.2	10	<0.1	26
2	CF_3SO_3H	−15	100	19	0	4.3	20	7.9	49
3	HCl	−8	100	13	4.0	5.0	14	2.2	62
4	H_2SO_4	−3	100	11	10	4.1	6.6	0.7	67
5	Oxalic acid	1.2	100	6.2	33	16	26	4.1	14
6	H_3PO_3	1.3	100	19	8.4	4.0	13	2.3	54
7[c]	H_3PO_3	1.3	100	5.3	16	8.1	25	2.1	43
8[d]	H_3PO_3	1.3	100	25	3.1	1.6	14	3.1	53
9	2,4-DNBA[e]	1.4	100	9.3	19	6.1	24	5.1	37
10	H_3PO_4	2.1	100	12	7.2	4.5	8.8	2.0	65
11	Malic acid	2.8	100	0.8	18	10	29	0.1	42

[a]S/C =2.0, 150 °C, 3 h, atmospheric pressure, no solvent. [b]AHADS: anhydro-ADS. [c]Diethyl ether was used for the impregnation of H_3PO_3 on ADS. [d]S/C = 4.0, 130 °C, 3 h, pressure <0.1 kPa. [e]2,4-Dinitrobenzonic acid.

yield of ADI increased to 25% at S/C 4.0, temperature 130 °C and pressure <0.1 kPa (entry 8). Under the optimised reaction conditions, we have confirmed that H_3PO_3 is more active than oxalic acid, 2,4-DNBA and H_3PO_4, and as active as CF_3SO_3H (Table S2).

Product mixtures dissolved in water after the dehydration of ADS usually have dark yellow to brown colours due to humin formation. After the reactions under the optimised conditions (Table S2), CF_3SO_3H gave a product solution with brown colour as expected (Fig. 2A). 2,4-DNBA and H_3PO_4 also afforded brownish colours, despite their low activity. However, H_3PO_3 and oxalic acid provided pale yellow solutions. UV-Vis spectra of the solutions were measured to know the source of the solution colours (Fig. 2B). We excluded 2,4-DNBA in the measurement, as this compound itself showed broad and strong UV absorption. Other acids had no absorption peaks at >230 nm, except for oxalic acid (240 nm). In a controlled experiment, a pure ADS solution gave a peak at <220 nm mainly derived from C=O π–π* transition. The absorption wavelength would not change significantly after the dehydration to monoanhydro-ADS or ADI. The reaction mixtures produced with CF_3SO_3H and H_3PO_4 provided additional peaks at 230–320 nm, which were ascribed to unsaturated bonds or conjugated systems such as furanics.[33] Dehydration of monoanhydro-ADS could produce furan derivatives and humins (Fig. S1). The shoulders of the absorption peaks for CF_3SO_3H and H_3PO_4 extended to the visible region (>380 nm), suggesting the presence of highly conjugated structures found in humins.[34] We have confirmed that a soluble humin material shows a broad absorption in the visible region (humic acid in Fig. 2B). Compared to the two acids, H_3PO_3 and oxalic acid gave smaller peaks for conjugated structures, thus leading to pale colours. Due to the reducing ability of H_3PO_3 and oxalic acid (eqs. 5, 6), they may be able to convert unsaturated chemical bonds to saturated ones in by-products.

$$H_3PO_4 + 2H^+ + 2e^- \rightleftarrows H_3PO_3 + H_2O \quad E^\circ = -0.276 \text{ V vs SHE} \quad (5)$$

$$2CO_2 + 2H^+ + 2e^- \rightleftarrows H_2C_2O_4 \quad E^\circ = -0.475 \text{ V vs SHE} \quad (6)$$

Related to the reducing ability, H_3PO_3 and oxalic acid decreased the formation of intermolecular condensation products leading to humin formation. SEC analysis (Fig. S2, Table S3) demonstrated that H_3PO_3 and oxalic acid produced intermolecular condensation products (molecular weight > 300) in peak area ratios of 36% and 10%, respectively. These ratios were lower than those given by CF_3SO_3H (62%), 2,4-DNBA (60%) and H_3PO_4 (53%). As unsaturated chemical bonds are reactive to produce condensation products,[35] reduction of the unsaturated groups possibly decreases the side-reactions. As humins prone to adhering to reactors,[36] the decrease in the amount makes process operation easier.

For a better understanding of the roles of H_3PO_3 in ADS dehydration, we studied the time course of the reaction (Fig. 3A). Yields of 1,4- and 3,6-anhydro-ADS were maximised at 0.5 h and afterwards gradually decreased by consecutive reactions. 1,5-Anhydro-ADS was similarly produced, but it decreased slowly after 1 h. ADI increased in a sigmoidal curve, and the

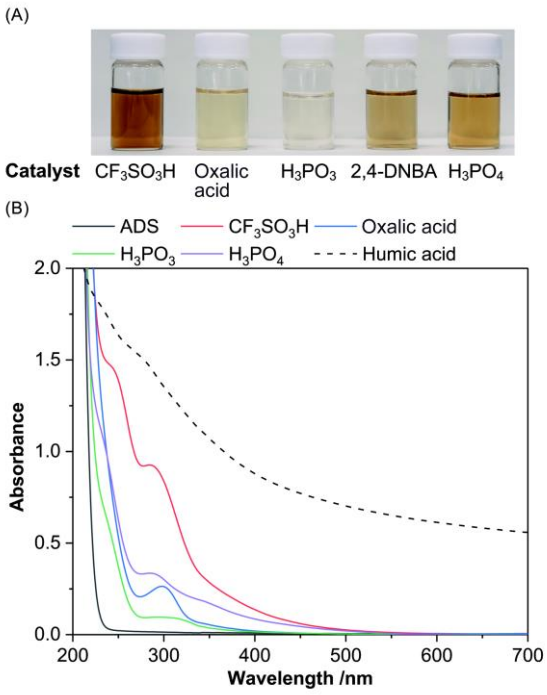

Fig. 2 (A) Photographs of aqueous solutions of products after the dehydration of ADS catalysed by CF_3SO_3H, oxalic acid, H_3PO_3, 2,4-dinitrobenzoic acid (2,4-DNBA) and H_3PO_4. (B) UV-Vis spectra of the solutions, ADS and humic acid.

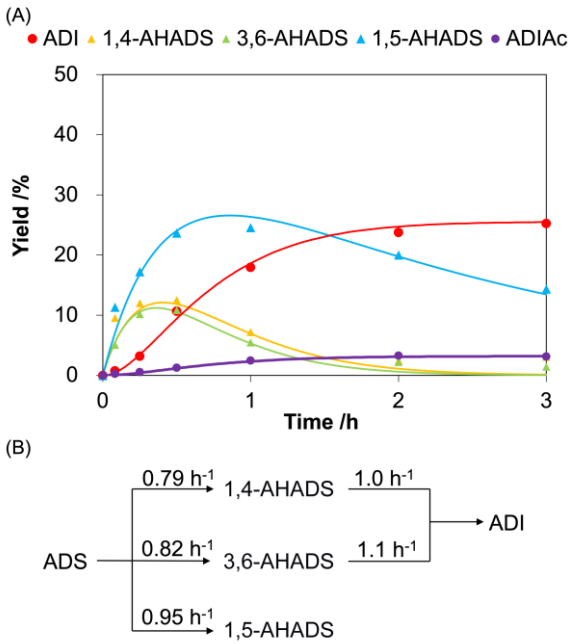

Fig. 3 (A) Time course of ADS dehydration by H_3PO_3 and (B) pseudo first-order rate constants obtained by the curve fitting. AHADS: anhydro-ADS. In (A), the plots indicate actual experimental results, and the lines show theoretical yield curves based on the kinetic analysis. Rate constants for the formation of other by-products from ADS, 1,4-AHADS, 3,6-AHADS and 1,5-AHADS were 0.30 h^{-1}, 1.30 h^{-1}, 1.80 h^{-1} and 0.38 h^{-1}, respectively.

yield reached 25% at 3 h. This profile demonstrates that ADI forms by successive reactions via 1,4- and 3,6-anhydro-ADS. A first-order approximation, often employed for the dehydration of sugar alcohols,[37-39] well reproduced the experimental data (solid lines in Fig. 3A). The formation of 1,4- (k = 0.79 h^{-1}), 3,6- (0.82 h^{-1}) and 1,5-anhydro-ADS (0.95 h^{-1}) took place with similar rate constants (ratio 31:32:37), which resembled those of CF_3SO_3H (29:31:40) and H_3PO_4 (30:33:37, Fig. S3). However, the rate constants for the dehydration of 1,4- and 3,6-anhydro-ADS to ADI (1.0 and 1.1 h^{-1}) were larger than those of the first step. This is surprising because the second dehydration is the rate-determining step for other acid systems (e.g., Fig. S3).[16]

The kinetic analysis has demonstrated the unique activity of H_3PO_3. The high activity cannot be explained on the basis of acid strength (H_3PO_3: pK_a 1.3), because oxalic acid (1.2) and 2,4-DNBA (1.4) were significantly less active than H_3PO_3 regardless of the similar acidity as shown in Table 1. To clarify the mechanism, we detected reaction intermediates with an LC/MS. The product mixture in a short-time ADS dehydration by H_3PO_3 (1 h, S/C = 4.0, 130 °C, pressure <0.1 kPa) showed large peaks at m/z = 250 and 268 at 10 min of retention time (Fig. S4B) and a small one at m/z = 286 at 22 min (Fig. S4C). The former peaks are assignable to phosphite esters of anhydro-ADS ($[M-H_2O-H]^-$, m/z = 250; $[M-H]^-$, m/z = 268), possibly mixed with the ester of ADI ($[M-H]^-$, m/z = 250). The latter (286) is attributable to the ester of ADS ($[M-H]^-$).

The LC/MS analysis motivated us to measure ^{31}P NMR of each fraction (Fig. S5). The fraction at 10 min gave several peaks in the range of 6.0–8.0 ppm in addition to the peak of H_3PO_3 at 4.6 ppm, while that at 22 min provided no peak due to low concentration of the product even accumulating the HPLC fraction for three days. For the 10-min fraction, the analytical assignment of the NMR peaks was difficult. Instead, we predicted ^{31}P NMR chemical shifts of phosphite esters using a quantum chemical calculation method as shown in Experimental (eq. 1). After determining the coefficients a and b as −0.457 and 141.2 by using three commercial phosphite esters (Fig. S6), the values were applied to estimate the chemical shifts of ^{31}P for phosphorous acid esters of 1,4-anhydro-ADS and 3,6-anhydro-ADS (Table 2). For convenience, the compounds are denoted 1,4- and 3,6-AHADS-nP, where n indicates the ester position. The calculation predicted peaks in the range of 6–8 ppm, which was roughly the same as those observed in the actual experiment (6–8 ppm). Hence, based on the LC/MS and NMR analyses, we conclude that the reaction contains anhydro-ADS phosphites.

Table 2 Computed shielding constants and predicted chemical shifts of phosphites.

Compound	σ_{calc} /ppm	δ_{pred} /ppm
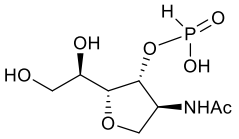 1,4-AHADS-3P	293.1	7.3
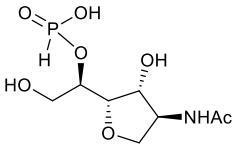 1,4-AHADS-5P	291.2	8.2
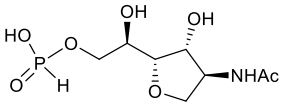 1,4-AHADS-6P	293.4	7.2
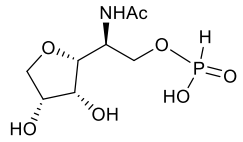 3,6-AHADS-1P	295.6	6.2
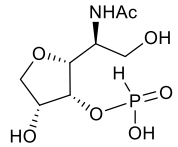 3,6-AHADS-4P	295.6	6.1
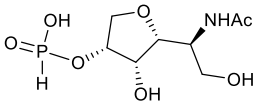 3,6-AHADS-5P	291.5	8.0

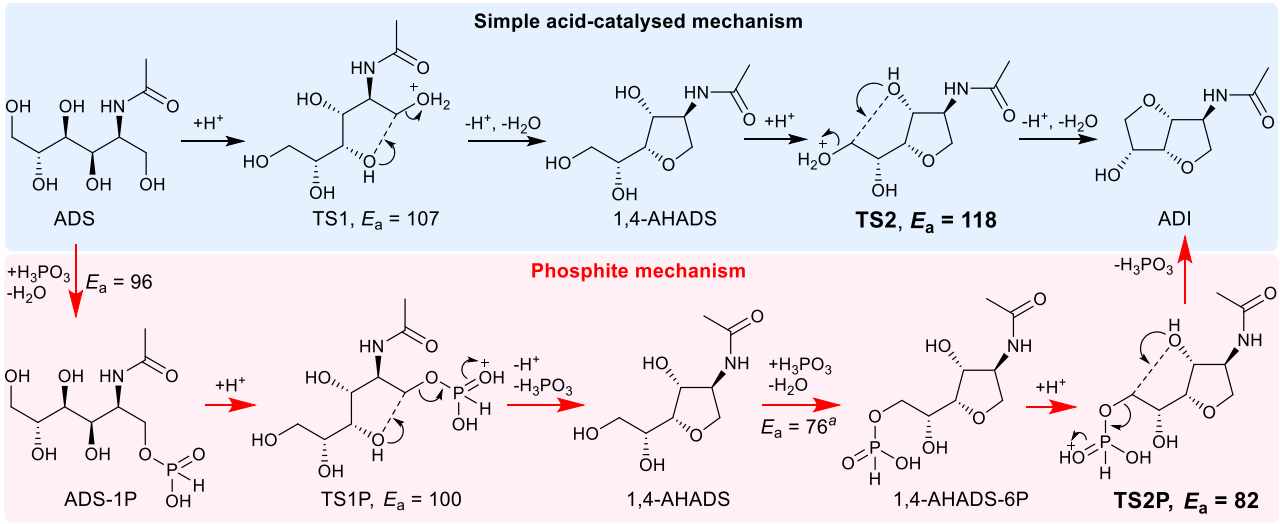

Fig. 4 Speculated reaction pathways for conversion of ADS to ADI. AHADS: anhydro-ADS. Activation energy (E_a) is in kJ mol^{-1}, determined by DFT calculations at the B3LYP/6-31+G(d,p) level with SMD. Protonation needs the deprotonation of H_3PO_3 as the counterpart. For the reaction, we assumed the following equation due to a high concentration of the acid (S/C 2–4): $2H_3PO_3 \rightarrow H^+ + [H_2PO_3 \cdots H_3PO_3]^-$. Even if deprotonation energy is changed, all E_a shift in parallel. [a]Esterification of 1,4-AHADS needs an additional amide compound to abstract a proton from H_3PO_3 (Fig. S7).

For the conversion of ADS to ADI by H_3PO_3, we anticipated a reaction pathway different from the common acid mechanism (Fig. 4). A typical acid-catalysed reaction occurs by protonation of a hydroxy group and subsequent dehydration cyclisation (Simple acid-catalysed mechanism; black arrows). In this reaction, hydroxy groups are less basic than the amide group, and therefore the amide group traps proton to slow down the reaction.[16] Alternatively, H_3PO_3 possibly forms esters at the primary positions, and then the P=O moiety is protonated (Phosphite mechanism; red arrows). Afterwards, H_3PO_3 works as a leaving group for the cyclisation.

To verify the possibility of this hypothesis, we conducted DFT calculations to determine the energy profiles of the respective reaction pathways. We employed B3LYP/6-31+G(d,p) with a solvent effect considered by SMD, which reasonably reproduced profiles of the dehydration of sugar alcohols in the previous studies.[16,20]

For the simple acid-catalysed reaction (Fig. 4; more detailed scheme Fig. S7), the amide moiety of ADS is protonated by H_3PO_3. Afterwards, the proton is transferred to a primary hydroxy group, leading to a transition state of dehydration cyclisation (TS1) with the activation energy (E_a) of 107 kJ mol^{-1}. The dehydration of 1,4-anhydro-ADS to ADI gives a higher E_a of 118 kJ mol^{-1} (TS2).

For the phosphite pathway, the esterification of ADS produces ADS-1P with a reasonable E_a of 96 kJ mol^{-1}. The reaction is energetically favoured, ΔE = −10 kJ mol^{-1} (see Fig. S7B), and ADS-1P is 10 to 30 kJ mol^{-1} more stable than the esters produced at secondary hydroxy groups. Therefore, we can expect the formation of ADS-1P. The ester captures a proton between C=O and P=O groups, and then an S_N2 reaction with eliminating H_3PO_3 generates 1,4-anhydro-ADS with an E_a of 100 kJ mol^{-1} (TS1P). More importantly, 1,4-AHADS-6P similarly converts to ADI with an E_a of only 82 kJ mol^{-1} (TS2P), after producing the ester with an E_a of 76 kJ mol^{-1}. Accordingly, H_3PO_3 can create a new reaction pathway via esters with low activation energies, which remarkably facilitates the step of converting 1,4-anhydro-ADS to ADI. The DFT calculations show that the P=O moiety in 1,4-AHADS-6P has a proton affinity ($\Delta H°$) of 1066 kJ mol^{-1}, which is higher than that of the primary OH group in 1,4-anhydro-ADS (1024 kJ mol^{-1}). The good basicity of P=O enables easy protonation of the P=O moiety to decrease E_a.

Conclusions

We have studied the dehydration condensation of ADS to ADI by weak acid catalysts. H_3PO_3 shows exceptionally high catalytic activity among weak acids tested. Additionally, the reducing ability of H_3PO_3 likely decreases the colouring of the product and the formation of humins. Rate constants for the dehydration of anhydro-ADS to ADI are larger than those of ADS to anhydro-ADS. This kinetics is specific to H_3PO_3, as other acids give very low rate constants to the conversion of anhydro-ADS. As for the mechanism, LC/MS and NMR analyses have indicated that the reaction with H_3PO_3 contains phosphorous acid esters of anhydro-ADS. DFT calculations verify that the phosphites can be intermediates for a new reaction pathway with lower activation energies than those of the typical acid-catalysed dehydration condensation. P=O groups in the esters undergo easy proton addition owing to high basicity. The protonation leads to the cyclisation reaction. This pathway removes the predominant issue of the conventional acid catalyst systems that the amide groups of substrates trap protons of the acid catalysts. Therefore, H_3PO_3 characteristically shows high activity in the conversion of ADS to ADI. Consequently, the weak acid replaces CF_3SO_3H, the corrosive and expensive catalyst used in the previous works,

for the conversion of ADS to ADI. Our reaction system decreases the cost of ADI production and environmental load. We hope that the insights in this work assist in the utilisation of chitin and apply to other dehydration reactions for basic group-containing molecules.

Author Contributions

C.Y.: Investigation, Formal Analysis, Data curation, Visualisation, Methodology, Writing – original draft. T.S.: Investigation, Methodology, Formal Analysis, Funding acquisition. A.F.: Conceptualization, Supervision, Validation, Resources, Writing – review & editing. H.K.: Conceptualization, Funding acquisition, Investigation, Methodology, Project administration, Resources, Validation, Visualisation, Writing – original draft, Writing – review & editing.

Conflicts of interest

There are no conflicts to declare.

Acknowledgements

This work was supported by Grant-in-Aid for Scientific Research (B) (18H01781; 21H01973) and for Young Scientists (19K15608) from Japan Society for the Promotion of Science (JSPS). We utilised an NMR instrument in the Open Facility of Institute for Catalysis (ICAT), Hokkaido University.

Notes and references

1 S. K. Kim, *Chitin, Chitosan, Oligosaccharides and Their Derivatives: Biological Activities and Applications*, CRC Press, Boca Raton, 2010.
2 X. Chen, H. Yang and N. Yan, *Chem. Eur. J.*, 2016, **22**, 13402-13421.
3 M. Pelckmans, T. Renders, S. Van de Vyver and B. F. Sels, *Green Chem.*, 2017, **19**, 5303-5331.
4 K. Nagasawa, Y. Tohira, Y. Inoue and N. Tanoura, *Carbohydr. Res.*, 1971, **18**, 95-102.
5 M. Yabushita, H. Kobayashi, K. Kuroki, S. Ito and A. Fukuoka, *ChemSusChem*, 2015, **8**, 3760-3763.
6 H. Kobayashi, K. Techikawara and A. Fukuoka, *Green Chem.*, 2017, **19**, 3350-3356.
7 G. Margoutidis, V. H. Parsons, C. S. Bottaro, N. Yan and F. M. Kerton, *ACS Sustainable Chem. Eng.*, 2018, **6**, 1662-1669.
8 H. Kobayashi, Y. Suzuki, T. Sagawa, K. Kuroki, J. Hasegawa and A. Fukuoka, *Phys. Chem. Chem. Phys.*, 2021, **23**, 15908-15916.
9 G. Gözaydın, S. Song and N. Yan, *Green Chem.*, 2020, **22**, 5096-5104.
10 X. Chen, Y. Liu, F. M. Kerton and N. Yan, *RSC Adv.*, 2015, **5**, 20073-20080.
11 M. Osada, K. Kikuta, K. Yoshida, K. Totani, M. Ogata and T. Usui, *Green Chem.*, 2013, **15**, 2960-2966.
12 D. Padovan, H. Kobayashi and A. Fukuoka, *ChemSusChem*, 2020, **13**, 3594-3598.
13 J. He, L. Chen, S. Liu, K. Song, S. Yang and A. Riisager, *Green Chem.*, 2020, **22**, 6714-6747.
14 T. T. Pham, X. Chen, T. Söhnel, N. Yan and J. Sperry, *Green Chem.*, 2020, **22**, 1978-1984.
15 F. D. Bobbink, J. Zhang, Y. Pierson, X. Chen and N. Yan, *Green Chem.*, 2015, **17**, 1024-1031.
16 T. Sagawa, H. Kobayashi, C. Murata, Y. Shichibu, K. Konishi and A. Fukuoka, *ACS Sustainable Chem. Eng.*, 2019, **7**, 14883-14888.
17 F. Fenouillot, A. Rousseau, G. Colomines, R. Saint-Loup and J.-P. Pascault, *Prog. Polym. Sci.*, 2010, **35**, 578-622.
18 T. Setoyama, *Catal. Surv. Asia*, 2014, **18**, 183-192.
19 H. Kobayashi and A. Fukuoka, *Green Chem.*, 2013, **15**, 1740-1763.
20 T. Sagawa, H. Kobayashi and A. Fukuoka, *Mol. Catal.*, 2020, **498**, 111282.
21 W. J. Hehre, R. Ditchfield and J. A. Pople, *J. Chem. Phys.*, 1972, **56**, 2257-2261.
22 P. C. Hariharan and J. A. Pople, *Theor. Chim. Acta*, 1973, **28**, 213-222.
23 T. Clark, J. Chandrasekhar, G. W. Spitznagel and P. von Ragué Schleyer, *J. Comput. Chem.*, 1983, **4**, 294-301.
24 C. Lee, W. Yang and R. G. Parr, *Phys. Rev. B*, 1988, **37**, 785-789.
25 A. D. Becke, *J. Chem. Phys.*, 1993, **98**, 5648-5652.
26 A. V. Marenich, C. J. Cramer and D. G. Truhlar, *J. Phys. Chem. B*, 2009, **113**, 6378-6396.
27 K. Fukui, *J. Phys. Chem.*, 1970, **74**, 4161-4163.
28 T. Lu, Molclus program, Version 1.9.9.3, http://www.keinsci.com/research/molclus.html (accessed Feb. 12, 2021).
29 H. B. Schlegel, *J. Comput. Chem.*, 1982, **3**, 214-218.
30 K. Wolinski, J. F. Hinton and P. Pulay, *J. Am. Chem. Soc.*, 1990, **112**, 8251-8260.
31 M. P. Andersson and P. Uvdal, *J. Phys. Chem. A*, 2005, **109**, 2937-2941.
32 M. Tafazzoli and H. P. Ebrahimi, *Phosphorus, Sulfur, Silicon Relat. Elem.*, 2011, **186**, 1491-1500.
33 R. F. Raffauf, *J. Am. Chem. Soc.*, 1950, **72**, 753-755.
34 I. Van Zandvoort, Y. Wang, C. B. Rasrendra, E. R. H. Van Eck, P. C. A. Bruijnincx, H. J. Heeres and B. M. Weckhuysen, *ChemSusChem*, 2013, **6**, 1745-1758.
35 N. Shi, Q. Liu, H. Cen, R. Ju, X. He and L. Ma, *Biomass Convers. Biorefin.*, 2020, **10**, 277-287.
36 Y. Nishimura, M. Suda, M. Kuroha, H. Kobayashi, K. Nakajima and A. Fukuoka, *Carbohydr. Res.*, 2019, **486**, 107826.
37 H. Yokoyama, H. Kobayashi, J. Hasegawa and A. Fukuoka, *ACS Catal.*, 2017, **7**, 4828-4834.
38 A. Yamaguchi, N. Muramatsu, N. Mimura, M. Shirai and O. Sato, *Phys. Chem. Chem. Phys.*, 2017, **19**, 2714-2722.
39 M. Yabushita, H. Kobayashi, A. Shrotri, K. Hara, S. Ito and A. Fukuoka, *Bull. Chem. Soc. Jpn.*, 2015, **88**, 996-1002.